IOP Conf. Series: Journal of Physics: Conf. Series **917** (2017) 062031 doi:10.1088/1742-6596/917/6/062031

Optical absorption edge parameters of zirconium dioxide nanotubular structures

A V Kozhevina[1], A S Vokhmintsev[1], R V Kamalov[1], N A Martemyanov[1], A V Chukin[1] and I A Weinstein[1,2]
[1]Ural Federal University, NANOTECH Center, Ekaterinburg,620002, Russia
[2] Institute of Solid State Chemistry, Russian Academy of Sciences, Yekaterinburg 620990, Russia

Abstract. Nanotubular layer of zirconia with an thickness of 10 ± 1 μm and an outer/inner diameters of nanotubes of 80/60 ± 5 nm was synthesized by anodization in the electrolyte based on ethylene glycol with small amount of water and ammonia fluoride. It is shown that the obtained samples before and after annealing in air at 400 °C consist of 90 % and 79 % tetragonal, 10 % and 21 % monoclinic phases, respectively. Analysis of diffuse reflectance spectra showed that the thermal treatment leads to a decrease in concentration of surface Zr^{3+}-centers. Under the assumption of direct allowed transitions, the bandgap width was estimated to be E_g = 5.41 ± 0.01 eV and 5.66 ± 0.01 eV for as-grown and annealed samples, respectively.

1. Introduction

Self-organized nanotubular structures of metal oxides obtained by anodizing are promising matrices for gas sensors, solar cells, photochemical and photoelectrochemical cells [1, 2]. It is known [3] that ZrO_2 with the energy gap of E_g = 5 – 5.8 eV [1, 4, 5] has one the largest photocatalytic activity under UV exposure (254 nm) in the series of transition metal oxides. However, the photocatalytic efficiency of ZrO_2 under sunlight drops considerably in comparison, for example, to TiO_2 (E_g = 3.1 to 3.2 eV [6]) that limits its practical use.

Electrochemical oxidation of Zr is mainly carried out in the potentiostatic mode at a voltage of ≤ 120 V in both inorganic aqueous media [7] - sulfates [8, 9], phosphates [1] and their mixtures [10, 11], and organic electrolytes based on ethylene glycol [9, 12], glycerol [13], mixtures of glycerol and ethylene glycol [14], glycerol and formamide [14 – 16]. However, it remains unclear how the anodizing conditions have an effect on the defectiveness of the synthesized ZrO_2 nanotubular layers and, consequently, on photocatalytic properties of zirconia. At the same time, it is known that self-organized highly ordered nanotubular structures of TiO_2, obtained in organic electrolytes based on ethylene glycol with fluoride ions and subjected to thermal treatment, have more efficient electron transport and, as a result, exhibit higher photocatalytic activity [17].

During the excitation of the samples by photons with energy of $h\nu < E_g$ the main role in electron-hole pairs generation is played by impurities and/or intrinsic defects forming a system of allowed energy levels within the forbidden gap and distort the optical absorption edge [18, 19 – 21]. The surface states with uncompensated chemical bonds of metal atoms (for example, Zr^{3+}-ions) and oxygen vacancies in a different charge state (F-type centers) are the predominant defects for ZrO_2 nanostructures. For this reason, a thermal treatment of samples under oxidizing conditions can reduce the concentration of intrinsic defects influencing the optical absorption edge.

In despite of the considerable interest in zirconium dioxide in various structural and phase states [18, 12, 22 – 27], a knowledge about the absorption characteristics of anodized ZrO_2 in the region of the optical absorption edge [1, 10] is insufficient. As an example, the energies E_g = 4.8 [1] and 4.13 eV [10] corresponding to ZrO_2 nanotubes fabricated by anodization process are significantly different from the energies corresponding to nanopowders and thin films obtained by other methods [1, 4, 5].
Thus, the aim of this work was to study structural and optical features of the zirconia layers synthesized by anodization in an electrolyte based on ethylene glycol with fluorine ions using scanning electron microscopy, X-ray diffraction and diffuse reflection techniques.

2. Samples and experimental techniques

2.1 Synthesis of ZrO_2 nanotubular layers

Before the anodizing a 300 μm thick zirconium foil (99.6%) was treated with acetone, etched in a solution containing $HF/HNO_3/H_2O$ (1:6:20), washed with distilled water and dried in air. The electrochemical oxidation was carried out in a two-electrode cell with a thermostatic control. The cathode was a stainless steel plate. The anodization was conducted at a constant voltage of 50 V and a temperature of 20 °C for 9 hours in the solution of ethylene glycol containing 5 wt. % H_2O and 0.5 wt. % NH_4F. After anodization the samples was washed and dried in air. The thermal treatment of synthesized structures was performed in air at 400 °C for 1 h. Thus, as-grown (S1) and annealed (S2) samples of anodized zirconia were obtained.

2.2 Characterization

The surface morphology of the anodized ZrO_2 was studied using scanning electron microscopy (SEM) by CarlZeiss SigmaVP. Structural characterization of as-grown and annealed samples was performed on PANalytical X'Pert PRO MPD diffractometer with a copper anode using the Rietveld method. The scanning step was fixed at 0.05°.

2.3 Diffuse reflection spectroscopy

An investigation of the absorption properties at room temperature was carried out using a Shimadzu UV-2450 two-beam spectrometer and an ISR-2200 integrating sphere. Scanning was conducted in the range of 190-850 nm with a spectral slit width of 2 nm at a rate of 90 nm/min.

3. Results

3.1 SEM characterization

The SEM images of the surface and cleavage of sample S1 is shown in Figure 1. It can be note that the synthesized oxide layer consists of highly ordered nanotubes with an external 80 ± 5 nm and an internal 60 ± 5 nm diameters. Some tubes (Figure 1a) are closed, presumably by a barrier layer of metal oxide [6] or remnants of a loose precipitated zirconium hydroxide [8]. The layer thickness of nanotubular ZrO_2 is 10 ± 1 μm.

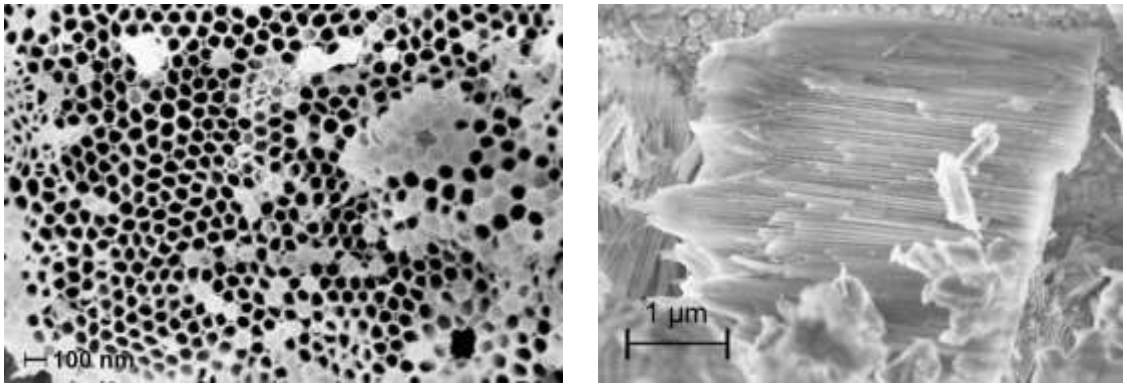

Figure 1. SEM images of surface (a) and lateral view (b) of anodized ZrO_2 layer.

3.2 XRD analysis

Figure 2 shows the XDR patterns of as-grown and annealed ZrO_2 samples. It can be seen that synthesized oxide layers have a crystalline structure. These spectra show characteristic peaks of both tetragonal (t) (scattering angles 2θ = 30.2, 50.2, 60.2, 74.5, 85.2°), and monoclinic (m) (at 2θ = 24.1, 28.2, 41.4, 55.9, 74.7, 83.1°) phases. The figure also presents the Zr peaks caused by the metal substrate.

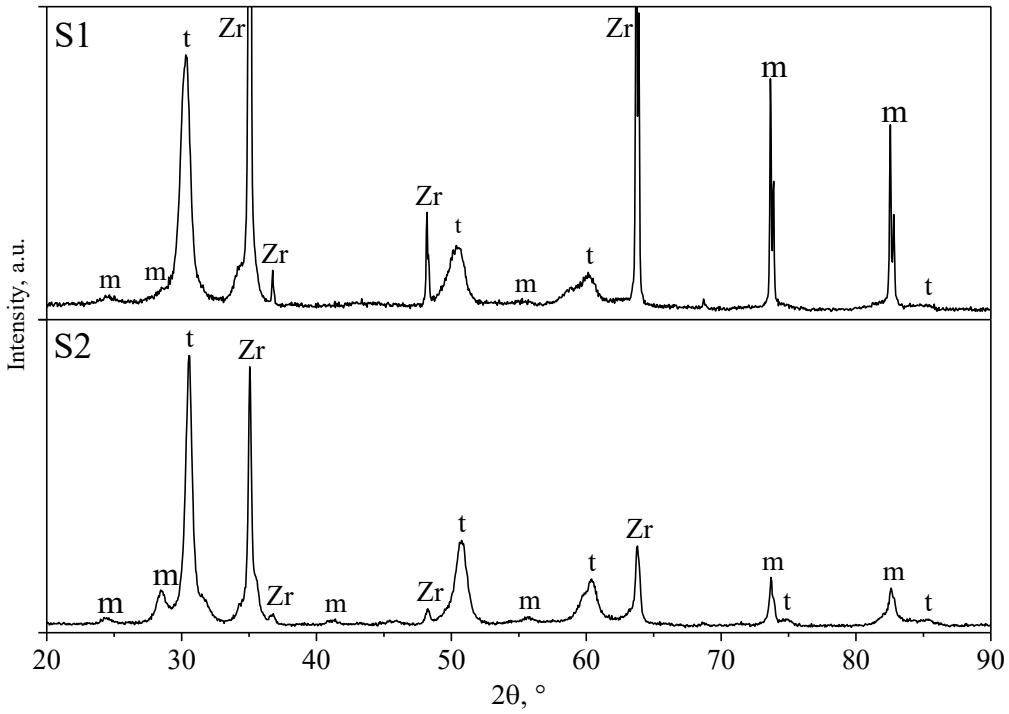

Figure 2. XRD patterns for as-grown (S1) and annealed (S2) samples.

3.3 Diffuse reflectance spectra

Figure 3 demonstrates the diffuse reflectance spectra $R(\lambda)$. It is seen that spectra have a sharp decline at $\lambda \leq 250$ nm due to the optical absorption edge. In the $\lambda = 250 – 850$ nm region, the R coefficient for the S2 sample is 5 to 15 % higher than for S1. This fact indicates the concentration decrease of the optically active color centers.

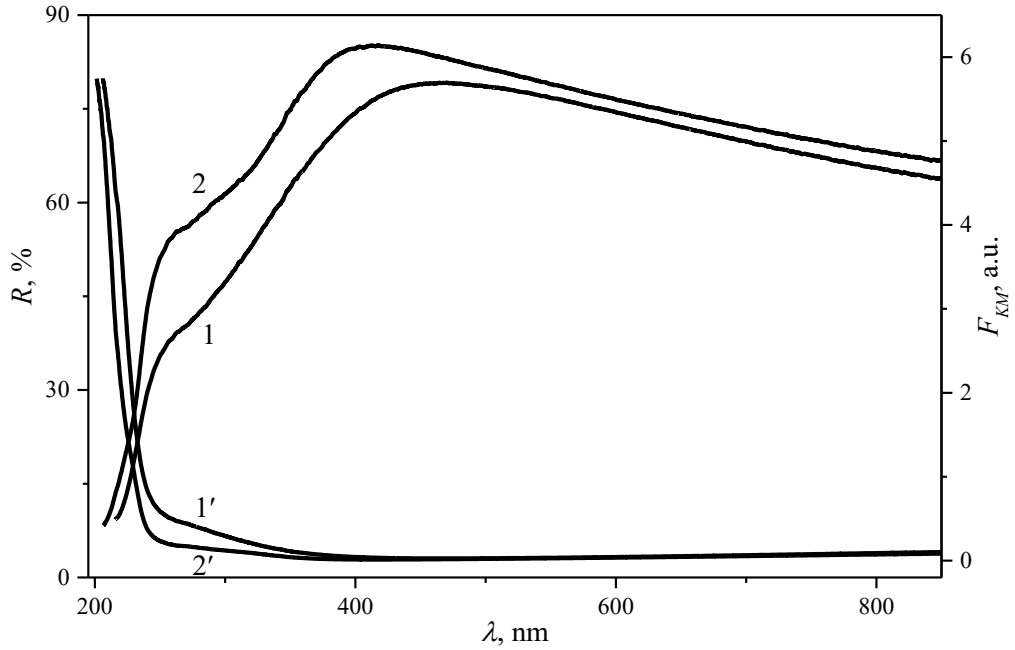

Figure 3. Diffuse reflectance spectra (1, 2 curves) and the Kubelka-Munk function (1′, 2′ curves) of S1 (1, 1′ curves) and S2 (2, 2′ curves) samples.

4. Discussion

A quantitative evaluation of the phase composition of the two-component system was carried out by a direct method. The experimental intensities of the main peaks for t- (30.2°) and m-ZrO2 (28.2°) were compared with the literature data. The 90 and 79 % of t-ZrO_2, 10 and 21 % of m-ZrO_2 were detected in samples S1 and S2, respectively. The obtained experimental data are in satisfactory agreement with studies of phase transformations in the low-temperature sintering process (200 – 350 °C) during the crystallization of an amorphous ZrO_2 nanopowder performed by decomposition of zirconium carbonate [28]. The authors of this work report that the crystallization proceeds with the formation of predominantly t- with the addition of m-ZrO_2 (15 – 20 %) with an average grain size of 36 ± 6 nm. It is also known that for macrosamples of ZrO_2 the phase transition of the monoclinic structure to the tetragonal one takes place at a temperature of 1170 °C [29]. In our case, the dominance of the tetragonal symmetry even in the as-grown samples and after annealing at 400 °C of ZrO_2 may exhibit the presence of structural features < 30 nm. This is consistent with the work data since the thickness of the zirconia nanotubes walls, according to SEM study, is near 20 nm, see 3.1.

For the analysis of the diffuse-reflectance spectra the Kubelka-Munk function was used, which is proportional to the optical absorption coefficient of the material:

$$F_{KM} = \frac{(1-R)^2}{2R} \quad (1)$$

where R is the diffuse reflection of the material measured with respect to the absolutely white body.

The calculated dependences of $F_{KM}(\lambda)$ are shown in figure 3, curves 1′ and 2′. Within the λ = 250 – 350 nm a shoulder is observed for the samples with clearer presence for the S1 structure. According to [18], the absorption band with a maximum at λ = 280 nm is due to Zr^{3+} centers. In this connection, it can be assumed that annealing in the air atmosphere leads to the oxidation of surface defects and, as a consequence, to bonds compensation and decrease in the concentration of Zr^{3+} centers.

The Tauc plot was used to determine the bandgap width [30] using:

$$\left(h\nu \cdot F_{KM}\right)^{1/n} = A\left(h\nu - E_g\right), \quad (2)$$

where n is a constant depending on the type of electronic transition in the material; A is a proportionality coefficient.

Analysis of the optical absorption spectra using expression (2) under the assumption of direct allowed transitions (n = 1/2) is shown in figure 4. Estimations of E_g for S1 and S2 samples were 5.41 ± 0.01 and 5.66 ± 0.01 eV, respectively. Obtained results are in satisfactory agreement with independent study of crystalline (E_g = 5.65 – 5.74 eV) and amorphous (E_g = 5.65 eV) zirconia films on Si-substrate obtained by magnetron sputtering [4] and atomic-layer deposition [5], respectively. However, for crystalline films of anodized ZrO_2, lower values of E_g = 4.8 [1] and 4.13 eV [10] are reported. This fact indicates a significant influence of the samples synthesis conditions on the characteristics of nanostructural ZrO_2 optical absorption edge.

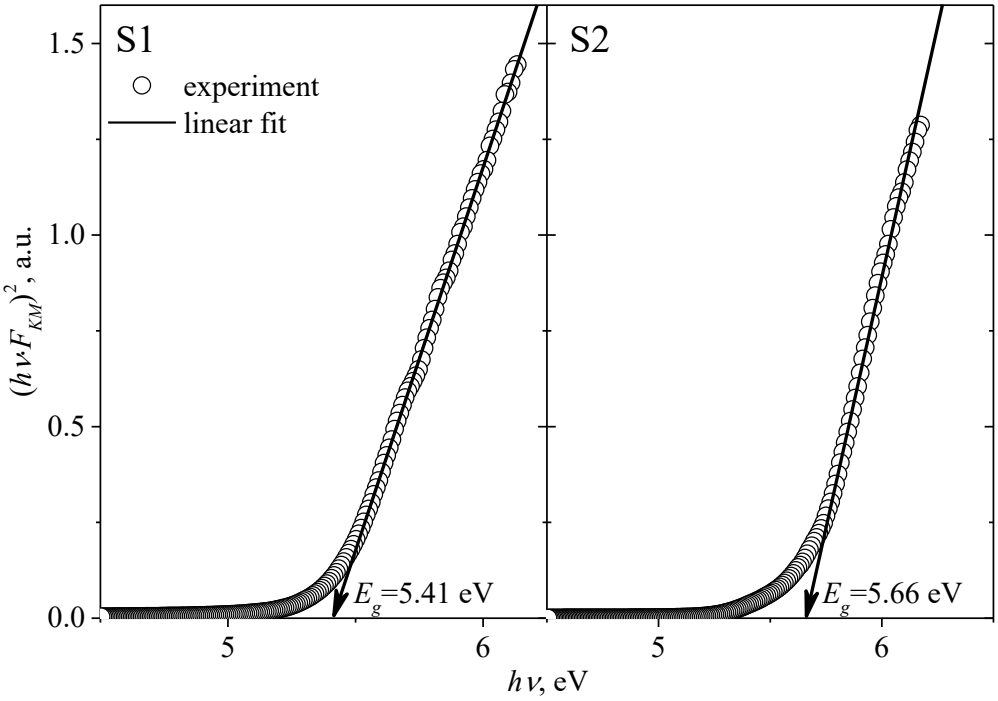

Figure 4. Tauc plot of optical absorption edge spectra for as-grown (S1) and annealed (S2) samples.

5. Conclusion

In the present research of nanotubular ZrO_2 samples synthesized by the anodic oxidation method was carried out. The morphology of the anodized oxide was studied by scanning electron microscopy. The thickness of the nanotubular layer was 10 ± 1 μm, the outer diameter of the nanotubes was 80 ± 5 nm, the inner diameter was 60 ± 5 nm. XRD analysis showed that as-grown samples and after 400 °C annealing consist of a mixture of tetragonal and monoclinic phases. The analysis of diffuse reflection spectra was performed. The bandgap width of E_g = 5.41 ± 0.01 and 5.66 ± 0.01 eV for nanotubular ZrO_2 samples before and after thermal treatment was determined under the assumption of direct allowed transitions using the Tauc plot. It was concluded that annealing of the investigated samples in the air atmosphere leads to compensation of break bonds of surface defects and a decrease in the concentration of Zr^{3+} centers.

Acknowledgments
The work was supported in part by Act 211 Government of the Russian Federation, contract № 02.A03.21.0006.

References
[1] Trivinho-Strixino F, Guimarães F E G and Pereira E C 2008 *Chem. Phys. Lett* **461** 82
[2] Kamalov R, Vokhmintsev A, Dorosheva I, Kravets N, Weinstein I 2016 *Adv. Sci. Lett* **22** 688
[3] Karunakaran C and Senthilvelan S 2005 *J. Mol. Catal. A-Chem* **233** 1
[4] Zhao S, Ma F, Xu K W and Liang H F 2008 *J. Alloy. Compd* **453** 453
[5] Puthenkovilakam R and Chang J P 2004 *Appl. Phys. Lett* **84** 1353
[6] Roy P, Berger S and Schmuki P 2011 *Angew. Chem.-Int. Edit* **50** 2904
[7] Lee W-J and Smyrl W H 2008 *Curr. Appl. Phys* **8** 818
[8] Tsuchiya H, Macak J M, Sieber I and Schmuki P 2005 *Small* **1** 722
[9] Tsuchiya H, Akaki T, Nakata J, Terada D, Tsuji N, Koizumi Y, Minamino Y, Schmuki P and Fujimoto S 2009 *Electrochim. Acta* **54** 5155
[10] Jiang W, He J, Zhong J, Lu J, Yuan S and Liang B 2014 *Appl. Surf. Sci* **307** 407
[11] Hahn R, Berger S and Schmuki P 2010 *J Solid State Electrochem* **14** 285
[12] Shin Y and Lee S 2009 *Nanotechnology* **20** 105301
[13] Muratore F, Baron-Wiecheć A, Hashimoto T, Skeldon P and Thompson G E 2010 *Electrochem. Commun* **12** 1727
[14] Berger S, Faltenbacher J, Bauer S and Schmuki P 2008 *Phys. Status Solidi-Rapid Res. Lett* **2** 102
[15] Fang D, Luo Z, Liu S, Zeng T, Liu L, Xu J, Bai Z and Xu W 2013 *Opt. Mater* **35** 1461
[16] Zhao J, Wang X, Xu R, Meng F, Guo L and Li Y 2008 *Mater. Lett* **62** 4428
[17] Kahnt A, Oelsner C, Werner F, Guldi D M, Albu S P, Kirchgeorg R, Lee K and Schmuki P 2013 *Appl. Phys. Lett* **102** 233109
[18] Emeline A, Kataeva G V, Litke A S, Rudakova A V, Ryabchuk V K and Serpone N 1998 *Langmuir* **14** 5011
[19] Ilin D O, Vokhmintsev A S and Weinstein I A. 2016 *AIP Conf. Proc* **1767** 020028
[20] Savchenko S S, Vokhmintsev A S and Weinstein I A 2017 *Opt. Mater. Express* **7** 354
[21] Savchenko S S, Vokhmintsev A S and Weinstein I A 2017 *Tech. Phys. Lett* **43** 297
[22] Liang J, Deng Z, Jiang X, Li F and Li Y 2002 *Inorg. Chem. Commun* **41** 3602
[23] Singh A K and Nakate U T 2014 *The Scientific World Journal* **2014** 349457
[24] Lucovsky G 2007 *J. Mol. Struct* **838** 187
[25] Rivera T, Olvera L, Azorín J, Sosa R, Barrera M, Soto A M and Furetta C 2006 *Radiat. Eff. Defects Solids* **161** 91
[26] Clament Sagaya Selvam N, Manikandan A, John Kennedy L and Judith Vijaya J 2013 *J. Colloid Interface Sci* **389** 91
[27] Nikiforov S V, Kortov V S, Savushkin D L, Vokhmintsev A S, Weinstein I A 2017 *Rad. Meas* in press DOI: 10.1016/j.radmeas.2017.03.020
[28] Gabelkov S V, Tarasov R V, Poltavcev N S, Logvinkov D S i Mironova A G 2004 *Voprosy atomnoj nauki i tekhniki* **3** 116 (in russian)
[29] Ackermann R J, Garg S P and Rauh E G 1977 *J. Am. Ceram. Soc* **60** 341
[30] Tauc J, Grigorovici R and Vancu A 1966, *Phys. Status Solidi B-Basic Solid State Phys.* **15** 627